Lift Hysteresis of an Oscillating Slender Ellipse

Mohammad A. Takallu*
Old Dominion University, Norfolk, Virginia
and
James C. Williams III†
Auburn University, Auburn, Alabama

A theoretical investigation has been conducted to determine the timewise variation of lift on a slender elliptic cylinder moving at uniform speed but oscillating in pitch. The analysis couples a potential flow calculation, including the effect of a vortical wake, for the flow past the cylinder with a calculation of the unsteady, two-dimensional, laminar boundary layer on the surfaces of the pitching ellipse. The coupling is achieved by matching the rate at which boundary-layer-developed vorticity is shed into the wake with the time rate of circulation about the ellipse. The unsteady lift is determined from an integration of the unsteady pressure distribution on the body. The effects of mean angle of attack and oscillation frequency on the lift hysteresis loops are determined. It is shown that the hysteresis loops change direction as the mean angle of attack is increased through the angle of attack corresponding to maximum steady lift.

Nomenclature

a = semimajor axis of ellipse; also radius of the mapping circle, m
b = semiminor axis of the ellipse, m
C_ℓ = unsteady lift coefficient
C_p = unsteady pressure coefficient
k = strength of the vortex
$q(t)$ = scaling functions as defined by Eq. (14)
Q_i = functions used in Eqs. (30) and (31)
$R(\eta)$ = parameter relating the angular measure to the distance along the surface
t = nondimensional time
T_1, T_2 = test functions used to satisfy the unsteady circulation criteria; see Eqs. (34) and (35)
u = nondimensional boundary-layer velocity in the x direction, $\hat{u}/U_\infty$
u_δ = nondimensional potential flow velocity on the body surface
U = absolute velocity of a point on the body, Eq. (37)
U_∞ = reference or freestream velocity, m/s
x = nondimensional streamwise boundary-layer coordinate
X = nondimensional real axis of the complex Z plane, $\hat{X}/a$
$\hat{X}$ = real axis in the $\hat{Z}$ plane, m
$\tilde{X}$ = nondimensional vortex location in the Z plane
Y = nondimensional imaginary axis in the complex Z plane, $\hat{Y}/a$
$\hat{Y}$ = chordwise axis of the body in the $\hat{Z}$ plane, m
y = nondimensional boundary-layer coordinate normal to the body surface, $\hat{y}\sqrt{Re}/a$
$\hat{y}$ = boundary-layer normal coordinate
Z = nondimensional complex coordinate of the body, $\hat{Z}/a$
$\hat{Z}$ = coordinate in the $\hat{Z}$ plane, $\hat{X}+i\hat{Y}$, m
α = angle of attack
α_0 = mean angle of attack
β = fineness ratio of the elliptic cylinder, b/a
γ = strength of the vortex per unit length of the wake
$\Gamma(t)$ = nondimensional unsteady circulation, $\hat{\Gamma}/2\pi a U_\infty$
$\hat{\Gamma}$ = unsteady circulation, m^2/s
δ = boundary-layer thickness
δ^* = displacement thickness
${}^1\delta, {}^2\delta, {}^3\delta$ = components of the unsteady boundary-layer thickness
$\Delta\alpha$ = increment of angle of attack
ζ = coordinate of the mapping circle, $e^{i\eta}$
η = angular measure in the ζ plane
θ = momentum thickness
λ = boundary-layer shape factor
ξ = streamwise coordinate as defined by Eq. (13)
ξ_s = location of separation point in ξ coordinates
ρ = location of isolated vortex in the ζ plane
τ_w = wall shear
ϕ = angular location of isolated vortex in the ζ plane
ω = nondimensional oscillation frequency, $\hat{\omega}a/U_\infty$
$\hat{\omega}$ = frequency, rad/s

Subscripts

le = leading edge
te = trailing edge
0 = steady components
10 = unsteady components multiplying $\Delta\alpha\cos\omega t$
11 = unsteady components multiplying $\Delta\alpha\sin\omega t$

Introduction

THE problem of determining the forces and moments on a body undergoing an oscillating pitching motion while moving at a uniform velocity in an infinite fluid has been of interest for several years. In recent years this interest stemmed from the relation of this problem to problems encountered in helicopter blade aerodynamics[1-3] or in rotating compressors when the inlet flow is nonuniform.[4] In the case of unsteady flow (oscillating pitch), the variation of lift with angle of attack is significantly different in and near stall from the familiar variation of lift for steady flow. In the steady flow case, there is a drastic decrease in lift at angles of attack greater than the stall angle of attack whereas for unsteady oscillatory cases the experiments of Halfman et al.[5] indicate a maximum dynamic lift coefficient which is significantly larger

Received June 20, 1983; revision received Feb. 9, 1984.

*Visiting Assistant Professor, Department of Mechanical Engineering and Mechanics. Member AIAA.

†Professor and Head, Department of Aerospace Engineering. Associate Fellow AIAA.

than the $C_{l_{max}}$. Furthermore, for an airfoil oscillating in pitch, the lift curve describes a hysteresis loop which is quite large when the mean angle of attack is near that for maximum steady-state lift. The size and shape of lift hysteresis loops are a strong function of mean angle of attack, oscillation amplitude, and frequency.[6]

Several investigators have studied this problem employing techniques which are basically inviscid but which are coupled with empirical estimates of the viscous effects.[7,8] While these methods may be useful in making predictions of unsteady aerodynamic effects, they do not go to the root of the problem. Basically, stall is a phenomenon which is directly related to boundary-layer separation and a complete analysis of stall, either steady or unsteady, must include the effects of boundary-layer separation. Several investigators have modeled unsteady stall including the effects of boundary-layer development. Crimi[9] analyzed the flow about an airfoil undergoing unsteady motion by modeling the basic flow elements and considering interactions between the viscous and inviscid flows by an iterative process. His work is limited by a linearized description of the potential flow which is solved numerically for each time step by considering a distribution of source and sink singularities. Patay[10] used a boundary-layer analysis to study the effect of leading-edge separation on the delay of dynamic stall for pitching Joukowski airfoils. This study employs a momentum integral procedure but solves only a quasisteady description of the flow process. Moore[11] considered the problem of predicting the lift on a slender elliptic cylinder in a freestream which is oscillating in angle of attack. In addition to considering the case of a stationary cylinder in an oscillating stream, Moore simplified his analysis by limiting the problem to the case of maximum static lift and considering only small rates of change of incidence. By restricting his analysis to maximum steady-state lift, Moore eliminated the quasisteady variation in circulation. In the lift vs angle-of-attack curve, Moore obtained a hysteresis loop whose direction is counterclockwise, in contrast to the clockwise direction of the hysteresis loops obtained experimentally on cylinders of airfoil cross section at high angle of attack. Sears[12] reviewed Moore's work and suggested that further investigations of this type be made. Sears discussed the effects of Moore's assumptions and stated that ". . . the dominant effect in this hysteresis may arise from quasisteady terms that Moore eliminated by considering small perturbations from maximum lift."

Johnson[13] extended the work of Moore by determining the hysteresis loops on a 6:1 ellipse oscillating periodically while moving through a stationary fluid. Johnson's analysis was not limited to maximum steady-state lift and hence included the quasisteady variations in circulation. Johnson did not include in his analysis the effect of the trailing vortical wake which affects the potential flow and hence the boundary-layer development and separation.

In the present work the analysis of Johnson is extended to include the contribution due to an infinite vortical wake and examine the unsteady viscous flow about a 6:1 elliptic cylinder oscillating in pitch while moving at constant speed through a stationary fluid. The analysis couples an unsteady potential flow calculation, including the vortical wake, with calculation of the unsteady boundary-layer development on the upper and lower surfaces of the ellipse. The coupling is achieved by matching the rate of change of circulation to the rate at which boundary-layer-developed vorticity is shed into the wake. The unsteady pressure distribution is integrated to determine the unsteady lift.

The results, which are presented for a range of mean incidence angles and oscillation frequencies, describe the behavior of the unsteady boundary layer and illustrate dynamic stall, including lift hysteresis.

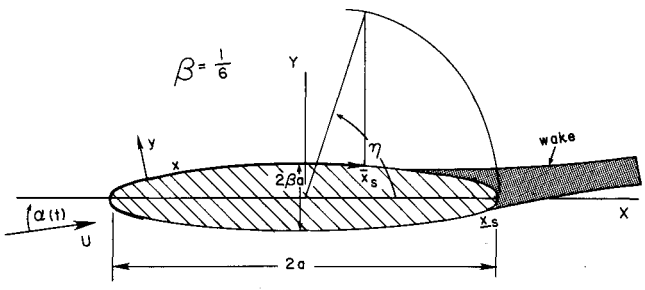

Fig. 1 Basic coordinate system and body orientation.

Analysis

The coordinate system and body orientation used in the present study are shown in Fig. 1. The x and y coordinates form the usual boundary-layer coordinate system. The x coordinate is measured from the stagnation point for steady flow at the mean angle of attack and is positive on the upper surface and negative on the lower surface. The angle η is measured positive counterclockwise from the trailing edge in a body-fixed coordinate system (X, Y). The angle of attack $\alpha(t)$ is assumed positive when the leading edge is pitched up relative to the direction of the relative freestream.

Potential Flow

The potential describing the fluid motion induced by an elliptic cylinder which is moving at constant speed through a stationary fluid while undergoing periodic changes in angle of attack may be obtained in the manner described by Kochin et al.[14] This complex potential is obtained by mapping the flow induced by a circle in the ζ plane into the flow induced by the ellipse in the z plane. The mapping between the two planes is given by

$$Z=\frac{1+\beta}{2}\zeta+\frac{1-\beta}{2}\frac{1}{\zeta} \tag{1}$$

However, the resulting potential does not include the effect of the periodic vortical wake. To model the contribution of the vortical wake, we begin by considering the contribution due to a single isolated vortex of strength k located at a point $\rho e^{i\phi}$ outside the cylinder in the ζ plane. The complex potential which describes this flow is given in Milne-Thomson.[15] The vortex is assumed to lie on the $\tilde{X}$ axis ($\phi=0$). The resulting potential is generalized by taking $k=\gamma(\tilde{X},t)\,d\tilde{X}$, where $\gamma(\tilde{X},t)$ is the vorticity per unit length in the wake. The contribution of the entire wake is then obtained by integrating from the trailing edge to infinity. The contribution of the shed vorticity between the separation point and the trailing edge has been neglected since this contribution will be small except in cases where separation moves quite far forward along the body. The total potential, including the effect of the vortical wake, is given by

$$w=\frac{1}{\zeta}(\beta\cos\alpha+i\sin\alpha)-\frac{i\Omega_z}{4\zeta^2}(1-\beta^2)$$
$$+i\Gamma\ln\zeta+i\int_{\tilde{X}_{te}}^{\infty}\left\{\ln\zeta+\ln(\zeta-\rho)-\ln\left(\zeta-\frac{1}{\rho}\right)\right\}\gamma\,d\tilde{X} \tag{2}$$

where

$$\rho=(1/1+\beta)\{\tilde{X}+\sqrt{\tilde{X}^2+\beta^2-1}\} \tag{3}$$

It is important to note that the total vorticity is made up of two parts: the vorticity "bound" in the ellipse which gives rise to the circulation Γ and the vorticity distributed in the wake. Since the total circulation about the combined system in-

cluding both the ellipse and the wake must be zero, we have

$$\Gamma+\int_{\tilde{X}_{te}}^{\infty}\gamma d\tilde{X}=0 \tag{4}$$

It is now assumed that the angle of attack varies periodically with time so that

$$\alpha=\alpha_0+\Delta\alpha\sin\omega t \text{ and } \Omega_z=-\frac{d\alpha}{dt}=-\omega\Delta\alpha\cos\omega t \tag{5}$$

Since the angle of attack varies periodically, it seems logical that the circulation should also vary periodically. Hence, we take

$$\Gamma=\Gamma_0+\Gamma_{10}\Delta\alpha\cos\omega t+\Gamma_{11}\Delta\alpha\sin\omega t \tag{6}$$

This form, containing both sine and cosine components, permits phase lead or lag in the final expression for the circulation. If the circulation Γ is periodic as a result of periodic variations in angle of attack, then it seems logical that the vorticity in the wake should be periodic also. If the motion has been occurring for a long period of time, it may be assumed that the transient phenomenon has vanished and the vortex strength in the wake is assumed to have the form:

$$\Gamma(\tilde{X},t)=A_R\cos(\omega t-\omega\tilde{X})+A_I\sin(\omega t-\omega\tilde{X}) \tag{7}$$

where $\tilde{X}=\hat{X}/a$. This particular distribution of vorticity corresponds to each element of trailing vorticity moving backward relative to the ellipse at a velocity U_∞. In the inertial frame of reference, the vorticity remains stationary in space as the airfoil moves away (forward) with a mean velocity, U_∞. For simplicity, the assumption is made that the vortices move at the freestream velocity relative to the ellipse. A more realistic assumption might be that the vortices move with a fraction of the freestream velocity. However, the value of this fraction is not known at this time.

Noting that the starting vortex cancels the steady-state circulation Γ_0, the coefficients A_R and A_I are determined from Eq. (4) so that

$$\gamma=\gamma_{10}\ \Delta\alpha\cos\omega t+\gamma_{11}\ \Delta\alpha\sin\omega t \tag{8}$$

where

$$\gamma_{10}=-\omega\{\Gamma_{10}\sin[\omega(\tilde{X}-\tilde{X}_{te})]+\Gamma_{11}\cos[\omega(\tilde{X}-\tilde{X}_{te})]\}$$

$$\gamma_{11}=\omega\{\Gamma_{10}\cos[\omega(\tilde{X}-\tilde{X}_{te})]-\Gamma_{11}\sin[\omega(\tilde{X}-\tilde{X}_{te})]\}$$

With the vorticity per unit length given by Eq. (8), the potential may be written, neglecting terms of order $(\Delta\alpha)^2$ and higher, as

$$w=\frac{1}{\zeta}(\beta\cos\alpha+i\sin\alpha)+i\Gamma_0\ln\zeta+\Delta\alpha\cos\omega t\left\{\frac{-2\omega(1-\beta^2)}{4\zeta^2}\right.$$

$$\left.+i\Gamma_{10}\ln\zeta+i\int_{\tilde{X}_{te}}^{\infty}\gamma_{10}\ln\left[\zeta\frac{(\zeta-\rho)}{[\zeta-(1/\rho)]}\right]d\tilde{X}\right\}$$

$$+\Delta\alpha\sin\omega t\left\{i\Gamma_{11}\ln\zeta+\int_{\tilde{X}_{te}}^{\infty}\gamma_{11}\ln\left[\zeta\frac{(\zeta-\rho)}{[\zeta-(1/\rho)]}\right]d\tilde{X}\right\} \tag{9}$$

The velocity may be obtained from the potential. Neglecting terms of order $(\Delta\alpha)^2$ and higher, the velocity on the body is

$$u_\delta(x,t)=u_{\delta_0}(x)+u_{\delta_{10}}(x)\Delta\alpha\cos\omega t+u_{\delta_{11}}(x)\Delta\alpha\sin\omega t \tag{10a}$$

in which

$$u_{\delta_0}(x)=(1/R)\{(1+\beta)\sin(\eta-\alpha_0)+\Gamma_0\} \tag{10b}$$

$$u_{\delta_{10}}(x)=(1/R)\{\Gamma_{10}(1-\omega Su)-\Gamma_{11}\omega Cu$$

$$-(\omega/2)[(1-\beta^2)\cos 2\eta+2\beta]\} \tag{10c}$$

$$u_{\delta_{11}}(x)=(1/R)\{\Gamma_{10}\omega Cu+\Gamma_{11}(1-\omega Su)$$

$$-(1+\beta)\cos(\eta-\alpha_0)\} \tag{10d}$$

where

$$Su=\int_{\tilde{X}_{te}}^{\infty}\left[1+\frac{1-\rho^2}{1+\rho^2-2\rho\cos\eta}\right]\sin[\omega(\tilde{X}-\tilde{X}_{te})]d\tilde{X}$$

$$Cu=\int_{\tilde{X}_{te}}^{\infty}\left[1+\frac{1-\rho^2}{1+\rho^2-2\rho\cos\eta}\right]\cos[\omega(\tilde{X}-\tilde{X}_{te})]d\tilde{X}$$

Here ρ is related to $\tilde{X}$ through Eq. (3) and η is related to the boundary-layer coordinate x by

$$\frac{dx}{d\eta}=-\frac{R(\eta)}{2} \tag{11}$$

If Γ_0, Γ_{10}, and Γ_{11} are prescribed, then one can determine the velocity potential from the complex potential and the velocity from Eqs. (10) and using these determine the pressure distribution on the body. The pressure distribution then can be integrated over the body to determine the force components and the pitching moment. For sharp trailing-edge airfoils at small angle of attack, Γ_0,Γ_{10}, and Γ_{11} are determined from the condition that the pressure difference between the upper and lower surfaces must approach zero as the trailing edge is approached (the Kutta condition). For sharp trailing-edge bodies at high angle of attack or blunt trailing-edge bodies, the boundary layer separates before the trailing edge and some other criterion must be used. For steady flow, the new criterion is the Taylor-Howarth criterion which requires that the net rate at which vorticity is shed into the wake be equal to zero. This criterion reduces to the usual Kutta condition at low angle of attack where separation does not occur. For unsteady flow the appropriate criterion is the revised Howarth-Taylor criterion advanced by Sears,[16] which requires that the time rate of change of circulation about the cylinder equal the net rate of vorticity flux into the wake. In order to apply this criterion, however, we must first calculate the boundary-layer development to separation on the top and bottom surfaces so that the rate of vorticity transport into the wake may be determined.

Boundary-Layer Development

In the present analysis the boundary-layer development is determined by employing an unsteady momentum integral technique to determine the location of the separation points. The standard unsteady momentum integral equations in nondimensional form is

$$\frac{\partial}{\partial t}(u_\delta\delta^*)+\frac{\partial}{\partial x}(u_\delta{}^2\theta)+u_\delta\delta^*\frac{\partial u_\delta}{\partial x}=\tau_w \tag{12}$$

in which δ^*, θ, and τ_w have their usual meanings, i.e.,

$$\delta^*=\int_0^\delta\left(1-\frac{u}{u_\delta}\right)dy,\quad \theta=\int_0^\delta\frac{u}{u_\delta}\left(1-\frac{u}{u_\delta}\right)dy,\quad \tau_w=\left.\frac{\partial u}{\partial y}\right|_{y=0}$$

As the body oscillates, the separation points on the upper and lower surfaces of the ellipse move back and forth. The present analysis accounts for this effect by transforming the momentum equation (12) with a scaling of the x coordinates so that the separation point always occurs at the same value of the new scaled coordinate. A brief discussion of the nature of unsteady boundary-layer separation is in order before such a transformation is developed.

It has been known for several years that the vanishing of the wall shear does not imply separation of the unsteady boundary layer. Moore,[17] Rott,[18] and Sears[12] independently postulated a model of unsteady separation (the MRS model) in which the unsteady separation point is characterized by the simultaneous vanishing of the velocity and shear at a point within the boundary layer, as seen by an observer moving with separation. Crimi[9] indicates that for a typical helicopter rotor Reynolds number and dimensionless pitch rate, the difference between the streamwise location of the separation point, as predicted by the MRS model and the location of the point of vanishing wall shear, is approximately 0.6% of the airfoil chord. This result, in addition to the physical reality that as the pitch rate approaches zero, the streamwise location of the unsteady separation point and the point of vanishing shear must coincide, leads to the adoption of vanishing wall shear as an adequate definition of the location of separation.

In order to scale the x coordinate in the desired fashion, the new coordinate ξ defined by

$$\xi = xq(t) \tag{13}$$

is introduced.

The scaling function $q(t)$ is chosen to have the form

$$q(t) = 1 + \Delta\alpha\{C_1 \cos\omega t + C_2 \sin\omega t\} \tag{14}$$

in which C_1 and C_2 are determined in order to insure that, to order $\Delta\alpha$, the separation point also occurs at a fixed value of ξ. With this scaling, the momentum integral equation becomes

$$\frac{\partial}{\partial t}(u_\delta\delta^*) + \frac{\xi}{q}\frac{dq}{dt}\frac{\partial}{\partial\xi}(u_\delta\delta^*) + q\frac{\partial}{\partial\xi}(u_\delta^2\theta) + qu_\delta\delta^*\frac{\partial u_\delta}{\partial\xi} = \tau_w \tag{15}$$

The technique employed herein to solve Eq. (15) is similar to that employed by Teipel[19] in a solution of the classical unsteady momentum integral equation. In order to extend the range of pressure gradients for which this procedure is applicable, a fifth-order polynomial similar to that employed by Dryden,[20] is employed to represent the velocity profile in the boundary layer. Thus, the general form of the u component of boundary velocity was assumed to be

$$\frac{u}{u_\delta(\xi,t)} = F(r) + \lambda G(r) \tag{16}$$

where $F(r)$ and $G(r)$ are fifth-order polynomials in $r = y/\delta$ given by

$$F(r) = \frac{17}{9}r - \frac{4}{3}r^3 + \frac{1}{9}r^4 + \frac{1}{3}r^5$$

$$G(r) = \frac{1}{7}r - \frac{1}{2}r^2 + \frac{9}{14}r^3 - \frac{5}{14}r^4 + \frac{1}{14}r^5$$

The coefficients in these polynomial expressions have been chosen in a manner similar to that employed by Dryden[20] so that the resulting steady-state lift curve was close to that obtained by a classical method while expanding the range of the shape factor which could be used.[20] It was further assumed that the boundary-layer thickness could be expanded in a series in $\Delta\alpha$, i.e.,

$$\delta(\xi,t) = \delta_0(\xi) + \delta_{10}(\xi)\Delta\alpha\cos\omega t + \delta_{11}(\xi)\Delta\alpha\sin\omega t \tag{17}$$

where $\delta_0(\xi)$ is given by the steady-state analysis and $\delta_{10}(\xi)$ and $\delta_{11}(\xi)$ are determined from the unsteady solution. Substituting gives the shape factor in expanded form as

$$\lambda = \lambda_0 + \lambda_{10}\Delta\alpha\cos\omega t + \lambda_{11}\Delta\alpha\sin\omega t \tag{18}$$

$$\lambda_0 = \delta_0^2\frac{du_{\delta 0}}{d\xi} \tag{19}$$

$$\lambda_{10} = \delta_0^2\frac{du_{\delta 10}}{d\xi} + \delta_0^2\omega\frac{u_{\delta 11}}{u_{\delta 0}} - \delta_0^2 C_1\xi\frac{d^2u_{\delta 0}}{d\xi^2} + 2\delta_0\delta_{10}\frac{du_{\delta 0}}{d\xi} \tag{20}$$

$$\lambda_{11} = \delta_0^2\frac{du_{\delta 11}}{d\xi} - \delta_0^2\omega\frac{u_{\delta 10}}{u_{\delta 0}} - \delta_0^2 C_2\xi\frac{d^2u_{\delta 0}}{d\xi^2} + 2\delta_0\delta_{11}\frac{du_{\delta 0}}{d\xi} \tag{21}$$

Further it is assumed that the displacement and momentum thicknesses and the wall shear can be expanded in series in $\Delta\alpha$ which to first order are:

$$\delta^* = \delta_0^* + \delta_{10}^*\Delta\alpha\cos\omega t + \delta_{11}^*\Delta\alpha\sin\omega t \tag{22}$$

$$\theta = \theta_0 + \theta_{10}\Delta\alpha\cos\omega t + \theta_{11}\Delta\alpha\sin\omega t \tag{23}$$

$$\tau_w = \tau_{w_0} + \tau_{w_{10}}\Delta\alpha\cos\omega t + \tau_{w_{11}}\Delta\alpha\sin\omega t \tag{24}$$

The components of the wall shear are given by

$$\tau_{w_0} = \frac{u_{\delta 0}}{\delta_0}\left(\frac{17}{9} + \frac{\lambda_0}{7}\right) \tag{25}$$

$$\tau_{w_{10}} = \frac{u_{\delta 0}}{\delta_0}\left\{\frac{\lambda_{10}}{7} + \left(\frac{17}{9} + \frac{\lambda_0}{7}\right)\left(\frac{u_{\delta 10}}{u_{\delta 0}} - \frac{\delta_{10}}{\delta_0}\right)\right\} \tag{26}$$

$$\tau_{w_{11}} = \frac{u_{\delta 0}}{\delta_0}\left\{\frac{\lambda_{11}}{7} + \left(\frac{17}{9} + \frac{\lambda_0}{7}\right)\left(\frac{u_{\delta 11}}{u_{\delta 0}} - \frac{\delta_{11}}{\delta_0}\right)\right\} \tag{27}$$

For future reference, note the requirement that the total shear vanish is satisfied if

$$\frac{17}{9} + \frac{\lambda_0}{7} = \lambda_{10} = \lambda_{11} = 0 \tag{28}$$

Finally, $u_{\delta 0}$, $u_{\delta 10}$, and $u_{\delta 11}$ are functions of x alone. These are written in terms of ξ by employing a Taylor series, e.g.,

$$u_{\delta_0}(x) = u_{\delta_0}\left(\frac{\xi}{1+\Delta\alpha q_1}\right) \simeq u_{\delta_0}[\xi(1-\Delta\alpha q_1)] \simeq u_{\delta_0}(\xi) - \Delta\alpha\xi q_1\frac{du_{\delta 0}}{d\xi}$$

using the assumed velocity distribution [Eq. (10a)]. The integral relations may be expanded as follows, neglecting terms of order $\Delta\alpha^2$.

Order $(\Delta\alpha)^0$:

$$(2\theta_0 + \delta_0^*)\frac{du_{\delta 0}}{d\xi} + u_{\xi 0}\frac{d\theta_0}{d\xi} = \frac{\tau_{w0}}{u_{\delta_0}} \tag{29}$$

Order $(\Delta\alpha)^1$:

$$\frac{d\delta_{10}}{d\xi}Q_1 + \delta_{10}Q_2 + \delta_{11}Q_3 + C_1Q_4 + C_2Q_5 - \omega\frac{du_{\delta 11}}{d\xi}Q_6 + \frac{du_{\delta 10}}{d\xi}Q_7 + u_{\delta_{10}}Q_8 + \omega u_{\delta_{11}}Q_9 - \frac{d^2u_{\delta 10}}{d\xi^2}Q_{10} = 0 \tag{30}$$

$$\frac{d\delta_{11}}{d\xi}Q_1 + \delta_{11}Q_2 - \delta_{10}Q_3 - C_1Q_5 + C_2Q_4 + \omega\frac{du_{\delta 10}}{d\xi}Q_6 + \frac{du_{\delta 11}}{d\xi}Q_7 + u_{\delta_{11}}Q_8 - \omega u_{\delta_{10}}Q_9 - \frac{d^2u_{\delta 11}}{d\xi^2}Q_{10} = 0 \tag{31}$$

The coefficients Q_1, Q_2, Q_3, ..., Q_{10} are easily calculated or may be found in Ref. 21. It should be noted that each of these coefficients is a function of the steady-state solution alone.

The reduced momentum equations, Eqs. (29-31), now could be solved in a prescribed fashion for δ_0^*, θ_0, τ_0, δ_{10}, and δ_{11} except that the unknown constants C_1 and C_2 appear in the equations for δ_{10} and δ_{11} [Eqs. (30) and (31)]. These constants are determined, as part of the solution process, from the requirement that the separation point be stationary in the moving coordinate system (in the body-fixed system, the separation point moves). This requirement is satisfied by making the total shear, given by Eq. (24), zero at the separation point $\xi = \xi_s$. This condition occurs when $\lambda_0 = -119/9$, and $\lambda_{10} = \lambda_{11} = 0$. Setting λ_{10} and λ_{11}, given by Eqs. (25) and (26), equal to zero at the separation point yields the two equations necessary for the determination of coefficients C_1 and C_2. The manner in which this determination is fitted within the solution procedure will be discussed shortly.

Circulation Criterion

Determination of the appropriate potential flow about the oscillating body involves specifying correct values of the unsteady circulation components in Eq. (6). As mentioned previously, the criterion used in the present study to determine values of Γ_0, Γ_{10}, and Γ_{11} was advanced by Sears.[12] The Taylor-Howarth criterion for determining the proper circulation in steady flow with separation requires that the net vorticity shed into the wake from both the upper and lower surfaces must be zero. Sears' modification of this requirement to account for unsteady effects, known as the revised Taylor-Howarth criterion, is given by

$$\frac{d\Gamma}{dt} = \text{rate of vorticity flux into the wake} \tag{32}$$

Allowing for the movement of the separation points, the criterion in Eq. (32) becomes

$$\frac{d\Gamma}{dt} = \frac{1}{2}\bar{u}_\delta^2 - \frac{1}{2}\underline{u}_\delta^2 + \underline{u}_\delta \frac{d\underline{x}_s}{dt} - \bar{u}_\delta \frac{d\bar{x}_s}{dt} \tag{33}$$

Table 1 Steady lift coefficient nondimensional steady circulation, and the location of the separation points for different mean angles of attack

α_0, deg	$\bar{\xi}_s$	ξ_s	Γ_0	C_{ℓ_0}
0	0.928	−0.928	0	0
2	0.894	−0.950	0.0250	0.159
4	0.840	−0.965	0.0490	0.324
6	0.740	−0.975	0.0695	0.466
7	0.655	−0.979	0.0768	0.491
8	0.526	−0.984	0.080	0.517
9	0.343	−0.989	0.0750	0.347

where the overbars and underbars denote conditions at separation on the upper and lower surfaces of the body, respectively. Changing the criterion in Eq. (33) to the (ξ, y, t) coordinate system yields the following three restrictions on Γ_0, Γ_{10}, and Γ_{11} when coefficients of 1, $\Delta\alpha \cos \omega t$, and $\Delta\alpha \sin \omega t$ are equated.

$$\bar{u}_{\delta_0}{}^2 = \underline{u}_{\delta_0}{}^2 \text{ at } \xi = \xi_s \tag{34}$$

$$T_1 = \omega\Gamma_{11} - \bar{u}_{\delta_0}\bar{u}_{\delta_{10}} + \xi_s \bar{C}_1 \bar{u}_{\delta_0} \frac{du_{\delta_0}}{d\xi}\bigg|_{\xi=\bar{\xi}_s} - \bar{C}_2 \bar{\xi}_s \omega \bar{u}_{\delta_0}$$

$$+ \underline{u}_{\delta_0}\underline{u}_{\delta_{10}} - \underline{\xi}_s \underline{C}_1 \underline{u}_{\delta_0} \frac{du_{\delta_0}}{d\xi}\bigg|_{\xi=\underline{\xi}_s} + \underline{C}_2 \underline{\xi}_s \omega \underline{u}_{\delta_0} = 0 \tag{35}$$

$$T_2 = -\omega\Gamma_{10} - \bar{u}_{\delta_0}\bar{u}_{\delta_{11}} + \xi_s \bar{C}_2 \bar{u}_{\delta_0} \frac{du_{\delta_0}}{d\xi}\bigg|_{\xi=\bar{\xi}_s} + \bar{C}_1 \bar{\xi}_s \omega \bar{u}_{\delta_0}$$

$$+ \underline{u}_{\delta_0}\underline{u}_{\delta_{11}} - \underline{\xi}_s \underline{C}_2 \underline{u}_{\delta_0} \frac{du_{\delta_0}}{d\xi}\bigg|_{\xi=\underline{\xi}_s} - \underline{C}_1 \underline{\xi}_s \omega \underline{u}_{\delta_0} = 0 \tag{36}$$

From Eq. (29), Γ_0 is determined by iteration until the velocity at the upper and lower separation points have equal magnitudes. To obtain correct values for the unsteady components of circulation, iteration is performed simultaneously on both Γ_{10} and Γ_{11} until Eqs. (35) and (36) are satisfied.

Solution Procedure

The preceding formulation allows the present problem to be solved in a pair of sequenced steps, each involving one or more iterative steps. The steady-state problem is solved first, and once it is known the unsteady portion of the problem is solved.

To solve the steady portion of the problem at a fixed steady mean angle of attack, α_0, a value of Γ_0 is first assumed. With α_0 and Γ_0 prescribed, the steady external velocity distribution u_{δ_0} is given [Eq. (10b)]. The boundary-layer development, to separation, on both the top and bottom surfaces is now determined. With the conditions at separation determined, a check is made of the separation criterion, Eq. (34). If the separation criterion is not satisfied, a new value of Γ_0 is assumed and the process outlined above is repeated. This procedure is repeated until one obtains a value of Γ_0 which satisfies the steady circulation criterion. By applying the scheme at successive angles of attack, one can generate the proper value of the steady-state circulation Γ_0, at each angle of attack, and, from this, as will be seen later, the steady-state lift curve.

Once Γ_0 has been found, the determination of Γ_{10} and Γ_{11} may begin. Here, however, there is a double iterative procedure since not only Γ_{10} and Γ_{11} but the unknown coefficients C_1 and C_2 must be determined. First test values of Γ_{10} and Γ_{11} are assumed. These values, together with the prescribed α_0 and the value of Γ_0 determined earlier, completely specify the

Table 2 Unsteady boundary-layer parameters, circulation components, and lift for several mean angles of attack and reduced frequencies

α_0	2 deg	6 deg	8 deg	8 deg	9 deg	9 deg
ω	0.1	0.01	0.1	0.01	0.1	0.01
$\bar{C}_1$	−0.2285	−0.7855	−2.2792	−0.2012	2.2783	3.2205
$\bar{C}_2$	1.2937	5.1176	19.3812	19.0100	51.7992	45.3325
$\underline{C}_1$	0.1237	0.033	0.01828	−0.0026	−0.1456	−0.0185
$\underline{C}_2$	−0.5895	−0.3965	−0.4834	−0.4489	−0.6225	−0.5421
Γ_0	0.025	0.0695	0.080	0.080	0.075	0.075
Γ_{10}	−0.058	−0.055	0.1525	0.0062	0.0355	0.0175
Γ_{11}	0.6435	0.449	−0.100	−0.0832	−1.247	−1.1139
C_{ℓ_0}	0.159	0.466	0.517	0.517	0.347	0.347
$C_{\ell_{10}}$	−0.137	−0.018	1.704	0.119	0.1289	−0.827
$C_{\ell_{11}}$	4.016	2.633	−4.357	−4.230	−21.35	−18.82

velocity distributions $u_{\delta 10}$ and $u_{\delta 11}$ [Eqs. (10c) and (10d)]. With these velocity distributions specified, the solution of Eqs. (30) and (31) for δ_{10} and δ_{11} is begun. These equations, however, contain the unknown constants C_1 and C_2. Because of the linearity of Eqs. (30) and (31), it is possible to split δ_{10} and δ_{11} into linear sums, i.e.,

$$\delta_{10} = {}^1\delta_{10} + C_1{}^2\delta_{10} + C_2{}^3\delta_{10}$$

$$\delta_{11} = {}^1\delta_{11} + C_1{}^2\delta_{11} + C_2{}^3\delta_{11}$$

Introducing these expressions into Eqs. (30) and (31) yields a set of six equations for the unknowns, ${}^1\delta_{10}$, ${}^2\delta_{10}$, ${}^3\delta_{10}$, ${}^1\delta_{11}$, ${}^2\delta_{11}$, and ${}^3\delta_{11}$. Four of these (the equations for ${}^2\delta_{10}$, ${}^3\delta_{10}$, ${}^2\delta_{11}$, and ${}^3\delta_{11}$) contain coefficients which depend only on the steady-state solution and, hence, may be solved once for all independently of the iterative process necessary to determine Γ_{10} and Γ_{11}. The remaining two equations (the equations for ${}^1\delta_{10}$ and ${}^1\delta_{11}$) involve $u_{\delta 10}$ and $u_{\delta 11}$ (and hence the assumed values of Γ_{10} and Γ_{11}).

The solutions for ${}^2\delta_{10}$, ${}^3\delta_{10}$, ${}^2\delta_{11}$, and ${}^3\delta_{11}$ are easily started employing standard procedures and are integrated using a fourth-order Runge-Kutta method. The equations for ${}^1\delta_{10}$ and ${}^1\delta_{11}$ require special attention in the vicinity of the stagnation point and are handled here in a manner which is based on Rott's[18] unsteady stagnation point solution. The unsteady motion of the stagnation point is then accounted for by employing Rott's technique, while the unsteady variation of the remainder of the boundary layer is accounted for by the transformation to the ξ coordinate. The two techniques are matched in the vicinity of the moving stagnation point. The details of the matching are given in Ref. 21. Once started, the equations for ${}^1\delta_{10}$ and ${}^1\delta_{11}$ are also solved by a fourth-order Runge-Kutta procedure. The solutions are all carried to the separation point. With ${}^1\delta_{10}$, ${}^2\delta_{10}$, ${}^3\delta_{10}$, ${}^1\delta_{11}$, ${}^2\delta_{11}$, and ${}^3\delta_{11}$ now determined, the unknown coefficients C_1 and C_2 are determined, as mentioned above, by requiring that the total shear, in the transformed coordinate ξ, vanish at the separation point. Then, by inserting the now known values of δ_0, δ_{10}, and δ_{11} evaluated at separation into Eqs. (20) and (21), and requiring that λ_{10} and λ_{11} vanish at separation [see Eq. (28)], one determines C_1 and C_2. With C_1 and C_2 defined, the assumed values of Γ_{10} and Γ_{11} are tested by determining if the circulation criteria, Eqs. (35) and (36), are satisfied. If these equations are not satisfied, new values of Γ_{10} and Γ_{11} are chosen and the entire process outlined above is repeated. This iteration process on Γ_{10} and Γ_{11} is repeated until the circulation criterion is satisfied. Because of space limitations, it has not been possible to describe this entire process in detail, or, in fact, that which follows. The details of the present analysis may be found in Ref. 21.

Upon completion of the above procedure, the unsteady circulation components Γ_0, Γ_{10}, and Γ_{11} have been determined for the body oscillating at a particular frequency about a prescribed angle of attack.

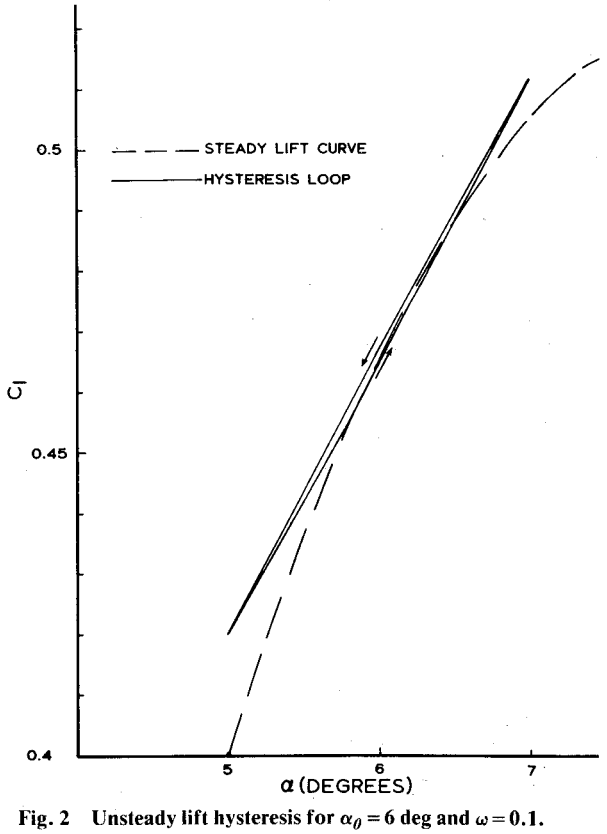

Fig. 2 Unsteady lift hysteresis for $\alpha_0 = 6$ deg and $\omega = 0.1$.

Aerodynamic Coefficient

The pressure on the surface of a cylinder in unsteady motion through an infinite fluid is given by the unsteady Bernoulli equation. Using this equation, the surface pressure coefficient is given by

$$C_p = \frac{p - p_\infty}{\rho U_\infty^2/2} = -2\frac{\partial \phi}{\partial t} + U^2(t) - u_\delta^2 \tag{37}$$

where U is the absolutely velocity of a point on the body, $u\delta$ the local velocity in the body-fixed coordinate system, and ϕ the velocity potential. The velocity potential is the real part of the complex potential equation (9) and the velocity u_δ is given by Eq. (10). The resulting expression for the pressure coefficient can then be written, again neglecting terms of $(\Delta\alpha)^2$ and higher, as

$$C_p = C_{p_0} + \Delta\alpha\, C_{p_{10}} \cos\omega t + \Delta\alpha\, C_{p_{11}} \sin\omega t \tag{38}$$

in which

$$C_{p_0} = 1 - u_{\delta_0}^2$$

$$C_{p_{10}} = -2\omega(1+\beta)\sin(\eta - \alpha_0) + 2\omega^2[\Gamma_{10} CNu - \Gamma_{11} SNu] + 2\omega\Gamma_{11}\eta - 2_{\delta_0} u_{\delta_{10}}$$

$$C_{p_{11}} = \omega^2 \frac{(1-\beta^2)}{2} \sin 2\eta + 2\omega^2[\Gamma_{10} SNu + \Gamma_{11} CNu] - 2\omega\Gamma_{10}\eta - 2u_{\delta_0} u_{\delta_{11}}$$

$$CNu(\eta) = \int_{\tilde{X}_{te}}^{\infty} \cos[\omega(\tilde{X} - 1)]\, \nu(\eta, \tilde{X})\, d\tilde{X}$$

$$SNu(\eta) = \int_{\tilde{X}_{te}}^{\infty} \sin[\omega(\tilde{X} - 1)]\, (\eta, \tilde{X})\, d\tilde{X}$$

$$\nu = \tan^{-1}\left[\frac{2\rho\sin\eta - \sin 2\eta}{2\rho\cos\eta - \cos 2\eta - \rho^2}\right]$$

This pressure coefficient, however, may be taken as representing only the pressure on that portion of the body for which the flow is attached. In order to integrate the pressure coefficient over the entire body to obtain lift, it is necessary to have some approximation for the pressure coefficient on the surface of the body in the separated region. In the present work the steady-state pressure coefficient C_{p_0}, beyond separation on the top surface, is assumed to decay exponentially to zero far behind the body, while the pressure coefficient beyond separation on the bottom surface is assumed to vary linearly from the pressure coefficient at separation to the value of the pressure coefficient obtained for

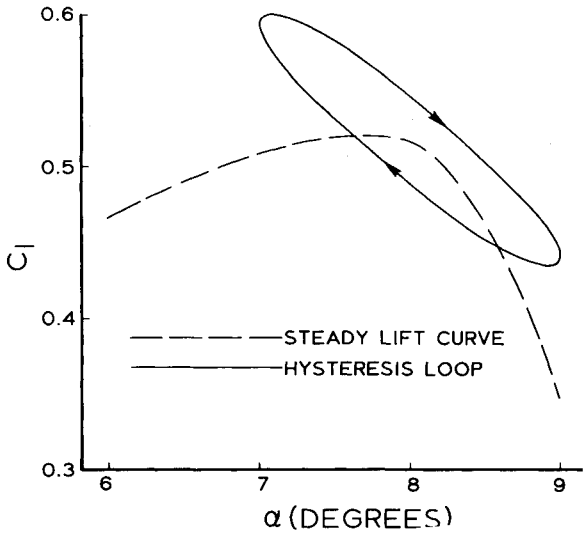

Fig. 3 Unsteady lift hysteresis near maximum lift ($\alpha_0 = 8$ deg) for $\omega = 0.1$.

the upper surface at the trailing edge of the ellipse. This procedure seems to provide reasonable results when applied to airfoils with separation where experimental data is available (e.g., see Ref. 22). The unsteady components of the surface pressure coefficients, $C_{p_{10}}$ and $C_{p_{11}}$, are assumed to vary linearly from their values (upper and lower surfaces) at separation to zero at the trailing edge, thus avoiding a pressure jump in the vortical wake.

With the pressure coefficients now completely determined, it is possible to integrate in a standard manner the pressure coefficient over the body surface to determine the lift. Quite obviously, the lift coefficient will have the form

$$C_\ell = C_{\ell_0} + \Delta\alpha\, C_{\ell_{10}} \cos \omega t + \Delta\alpha C_{\ell_{11}} \sin \omega t$$

Results and Discussion

The analysis described herein has been employed to predict the steady and unsteady lift coefficient components for an elliptic cylinder of fineness ratio 1:6 oscillating in pitch at a number of mean angles of attack. Calculations were performed for reduced frequencies of $\omega = 0.01$ and 0.1. Results are presented for a constant perturbation of the angle of attack of $\Delta\alpha = 1$ deg.

The steady-state lift coefficient was found for mean angles of attack from 0 to 9 deg. Table 1 presents values of Γ_0 and C_{ℓ_0} and the upper and lower separation points $\bar{\xi}_s$ and $\underline{\xi}_s$ for angles of attack from 2 to 9 deg. The steady-state lift coefficient increases with angle of attack up to an angle of attack of 8 deg where a maximum lift coefficient of $C_{\ell_0} = 0.517$ occurs. Beyond 8 deg, the lift drops off as the separation point moves forward along the body exposing a large portion of the upper surface to the separated wake. At 9 deg, separation occurs on the upper surface $\bar{\xi}_s = 0.343$ and on the lower surface at $\bar{\xi} = -0.989$, quite close to the trailing edge.

The major results obtained from these calculations are presented in Table 2. The resulting lift hysteresis loops are shown later Figs. 2 and 3. For $\alpha_0 = 2$ deg, the hysteresis loop appeared to be very thin and proceeded in a counterclockwise direction. The results for $\alpha_0 = 6$ deg, shown in Fig. 5, indicate that the hysteresis loop is still quite thin and there is no change in the direction. As the mean angle of attack is increased further to a value near the angle of attack for maximum steady-state lift, the viscous effect becomes more important with a resulting thickening of the hysteresis loop and a change in the direction and transversing the loop to clockwise (Fig. 3). Beyond the angle for maximum steady-state lift, at $\alpha = 9$ deg (not shown), the hysteresis loop becomes very thin again while the loop is still transversed in the clockwise direction.

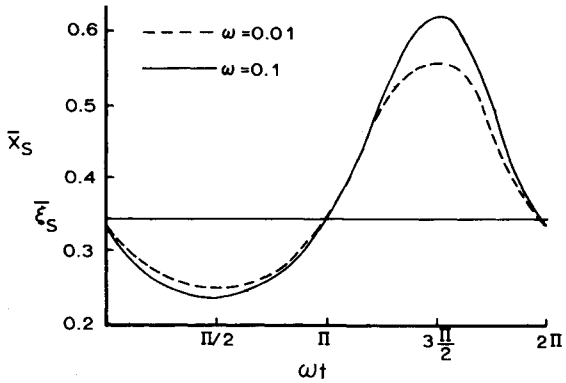

Fig. 4 Movement of upper separation point, $\alpha_0 = 9$ deg.

In general, these results for the direction of transversing the hysteresis loops are in agreement with the experimental results of Liiva et al.[6] for a two-dimensional airfoil oscillating in pitch. The experimental results of Liiva et al. indicate that at small angle of attack the hysteresis loop is counterclockwise, while beyond the angle for steady-state maximum lift the hysteresis loop is clockwise. The major difference between the present results and the experiments lies in the transition from counterclockwise to clockwise hysteresis loops. In the experiments this transition involves a shift from single counterclockwise loops to figure-eight loops with both clockwise and counterclockwise parts back to single clockwise hysteresis loops at high angles of attack. The present analysis, which contains only terms of order $\Delta\alpha$, cannot produce hysteresis loops of the figure-eight type.

The results presented herein, with respect to the direction of the hysteresis loops, are at variance with those of Johnson.[13] This is probably the result of including the effect of the vortical wake in the present analysis. In addition, the present results include a direct integration of the surface pressure to obtain lift, whereas Johnson[13] (and also Moore[11]) related the lift directly to the circulation. The direct relation of lift to circulation, as employed by Johnson[13] and Moore,[11] ignores the effect of boundary-layer separation and the pressure distribution in the separated region. In the present work, the integration of the surface pressure accounts, at least approximately, for the effect of the separated flow on the surface pressure and, hence, the lift.

In order to better understand the above results for the unsteady lift on an elliptical cylinder, Figs. 4 and 5 present an in-depth look at the various intermediate parameters which affect the lift. Figure 4 illustrates the movement of the separation point on the upper surface as $\alpha(t)$ completes a full cycle for a mean angle of attack of 9 deg. The movement of the upper separation point seems to be more sensitive to the unsteady oscillations than the one on the lower surface. The movement of the lower surface separation point is only about 20% of the movement of the upper surface separation point. For example, at a mean angle of attack of 9 deg the lower surface separation point moves between $x = 0.984$ and 0.995 during one cycle. This is also true for the variations with respect to the oscillation frequency ω. However, there is a phase shift present for both surfaces as $\omega = 0.1$ changes to $\omega = 0.01$.

In obtaining the velocity components at each point on the body, it was necessary to evaluate the contribution due to the vortical wake by carrying out an integration along the vortical wake [e.g., the integrals *Su* and *Cu* in Eqs. (10c) and (10d)]. It was found that it is necessary to carry this integration some 200 chord lengths along the wake before the integrals become essentially constant; i.e., additional contributions to the integral were on the order of 10^{-4}. If one were satisfied to

evaluate these integrals to, say, within 10% of the true value, it would be necessary to carry the integral out to approximately 50 chord lengths. The reason it is necessary to carry the integration so far lies in the fact that the effect of the vortical wake dies out, not as the inverse square of the distance from the trailing edge to the element of vorticity, but simply as the inverse of the distance. This is clearly shown in the expressions for Su and Cu [after Eqs. (10)] and from Eq. (3) which relates ρ to $\bar{X}$. Since the vorticity in the wake takes the form of a damped traveling wave, it is appropriate to consider the length of the wake in terms of wavelengths. The distance 200 chord lengths corresponds to 6.4 wavelengths for $\omega = 0.10$ and 0.64 wavelengths for $\omega = 0.01$. The above result indicates that components of the wake quite far from the body still exert a noticeable effect on the flow in the vicinity of the body. This, in turn, represents an inconvenience manifested in longer computing time.

The typical behavior of the unsteady pressure coefficient can be seen in Fig. 5 where the unsteady components of $C_p(t)$ are plotted as a function of ξ for a nominal value of $\alpha_0 = 9$ deg and $\omega = 0.1$. Here, the steady pressure coefficient on the upper surface decreases as the velocity increases around the nose, and then picks up toward the trailing edge. On the lower surface, C_{p0} decreases toward the trailing edge and experiences a sharp increase associated with an adverse pressure gradient necessary for the separation at the lower surface. Although somewhat different in magnitude, a similar behavior can be observed for the variation of C_{p10} and C_{p11} around the elliptic cylinder.

The results of the present investigation seem to support the following hypothesis made by Moore[11]: "It may be that different directions of hysteresis should be expected when the airfoil oscillates and when, as in the present study, the stream direction oscillates.[11] Indeed it appears that the clockwise direction of the hysteresis loop, which agrees with experimental airfoil results, is a direct consequence of including

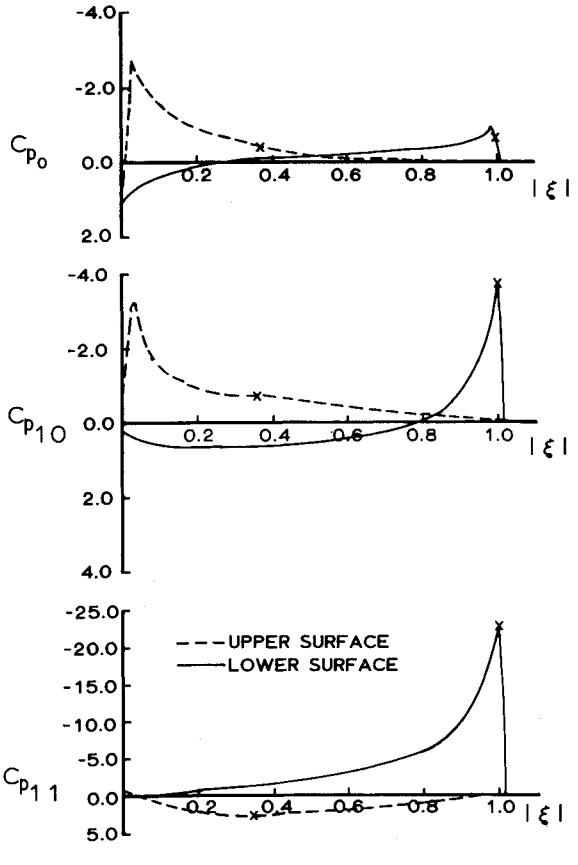

Fig. 5 Pressure distributions for $\alpha_0 = 9$ deg and $\omega = 0.1$.

the Ω_z term in the expression for $u_\delta(x,t)$ which alters the form of $u_{\delta 10}$ to produce a positive value of Γ_{10}. The Ω_z term arises as a result of the body oscillating as it translates through an infinite fluid. Setting this term equal to zero or neglecting it, as Moore[11] did, corresponds to the physically unrealistic case in which the body is stationary in an oscillating infinite medium. Physically, this additional term seems to describe the influence on the potential flow of the added mass effect associated with an accelerating body in unsteady motion. This result is in agreement with the results of Johnson,[13] although Johnson did not include the effect of the vortical wake.

Summary

An unsteady momentum integral technique has been employed to analyze the laminar, two-dimensional, unsteady boundary layer on an elliptic cylinder oscillating periodically in a steady freestream. The dynamic lift characteristics and the unsteady behavior of the boundary layer are predicted for several nominal angles of attack over a range of oscillation frequencies.

The basic approach was to represent the boundary-layer parameters by a steady-state term plus an unsteady perturbation proportional to $\Delta\alpha$, to transform the usual boundary-layer coordinate system such that the location of the separation points appear steady in the new coordinate system, and to relate the rate at which vorticity is shed into the wake to the time rate of change of circulation.

The predicted hysteresis loop direction was found to change from counterclockwise to clockwise as the mean angle of attack was increased from 2 deg to within the stall region. This direction change was shown to compare favorably with experimental results for cylinders of airfoil cross section.

References

[1] Ham, N. D. and Young, M. I., "Torsional Oscillation of Helicopter Blades Due to Stall," *Journal of Aircraft,* Vol. 3, March 1966, pp. 218-224.

[2] Young, W. H. Jr., "Fluid Mechanics Mechanisms in the Stall Process of Airfoils for Helicopters," *Numerical and Physical Aspects of Aerodynamic Flows,* edited by Tuncer Cebeci, Springer-Verlag, New York, 1982, pp. 601-615.

[3] McCroskey, W. J., McAlister, K. W., Carr, L. W., Pucci, S. L., Lambert, O., and Indegrand, R. F., "Dynamic Stall on Advanced Airfoil Sections, *Journal of the American Helicopter Society*, Vol. 26, No. 3, July 1981, pp. 40-50.

[4] Emmons, H. N., Kronauer, R. E., and Rockett, J. A., "A Survey of Stall Propagation—Experiment and Theory," *Transactions of ASME, Journal of Basic Engineering,* Ser. D, Vol. 31, 1959, pp. 409-416.

[5] Halfman, R. C., Johnson, H. C., and Haley, S. M., "Evaluation of High Angle-of-Attack Aerodynamic-Derivation Data and Stall-Flutter Prediction Techniques," NACA TN 2533, 1951.

[6] Liiva, J., Davenport, F. J., Lewis, G., and Walton, I. C., "Two-Dimensional Tests of Airfoils Oscillating Near Stall, Vol. 1, Summary and Evaluation of Results," U.S. Army Aviation Material Laboratories, Fort Eustis, Va., USAAVLABS Tech. Rept. 68-13A, 1968.

[7] Ham, N. D., "Aerodynamic Loading of a Two-Dimensional Airfoil During Dynamic Stall," *AIAA Journal,* Vol. 10, Oct. 1968, pp. 1927-1934.

[8] Ericsson, L. E. and Reding, J. P., "Dynamic Stall of Helicopter Blades," *Journal of the American Helicopter Society*, Vol. 17, Jan. 1972, pp. 11-19.

[9] Crimi, P., "Dynamic Stall," AGARD-AG-172, Langley Field, Va., 1973.

[10] Patay, S. A., "Leading Edge Separation on an Airfoil During Dynamic Stall," MIT Aero-Elastic and Structures Research Laboratory, Cambridge, Mass., ASRL TR 156-1, 1969.

[11] Moore, F. K., "Lift Hysteresis at Stall as an Unsteady Boundary Layer Phenomenon," NACA TN 3571, 1955.

[12] Sears, W. R., "Some Recent Developments in Airfoil Theory," *Journal of Aeronautical Science,* Vol. 23, No. 5, 1956, pp. 490-499.

[13] Johnson, D. A., "Unsteady Momentum Integral Analysis of the Laminar Boundary Layer on an Elliptic Cylinder Oscillating in Pitch," Ph.D. Thesis, North Carolina State University, Raleigh, N.C., 1974.

[14] Kochin, N. E., Kibel, I. A., and Roze, N. V., *Theoretical Hydromechanics,* John Wiley & Sons, Inc., New York, 1964.

[15] Milne-Thomson, L. M., *Theoretical Hydrodynamics,* The Macmillan Co., New York, 1965.

[16] Sears, W. R., "Unsteady Motion of Airfoils with Boundary Layer Separation," *AIAA Journal,* Vol. 14, Feb. 1976, pp. 216-220.

[17] Moore, F. K., "On the Separation of the Unsteady Laminar Boundary Layer," *Boundary Layer Research,* Springer-Verlag, Berlin, 1958, pp. 296-310.

[18] Rott, N., "Unsteady Flow in the Vicinity of a Stagnation Point," *Quarterly on Applied Mathematics,* Vol. 13, 1956, pp. 444-451.

[19] Teipel, I., "Calculation of Unsteady Boundary Layer by an Integral Method," *Zeitschrift der Flugwissenschaften,* Vol. 18, Heft 213, 1970, pp. 58-65.

[20] Dryden, H. L., "Computation of the Two-Dimensional Flow in a Laminar Boundary Layer," NACA TR 497, 1934, pp. 435-443.

[21] Takallu, M. A., "Lift Hysteresis for an Oscillating Elliptic Cylinder," Ph.D. Dissertation, Department of Mechanical and Aerospace Engineering, North Carolina State University, Raleigh, N.C., 1982.

[22] Fage, A., "The Flow of Air and of an Inviscid Fluid around an Elliptic Cylinder and an Airfoil of Infinite Span, Especially in the Region of the Forward Stagnation Point," *Philosphical Transactions of the Royal Society of London,* Ser. A, Vol. 227, 1928.